

Actively Stressed Marginal Networks

M. Sheinman,¹ C. P. Broedersz,² and F. C. MacKintosh¹

¹*Department of Physics and Astronomy, VU University, 1081 HV Amsterdam, The Netherlands*

²*Lewis-Sigler Institute for Integrative Genomics and the Department of Physics,
Princeton University, Princeton, New Jersey 08544, USA*

(Received 27 June 2012; published 3 December 2012)

We study the effects of motor-generated stresses in disordered three-dimensional fiber networks using a combination of a mean-field theory, scaling analysis, and a computational model. We find that motor activity controls the elasticity in an anomalous fashion close to the point of marginal stability by coupling to critical network fluctuations. We also show that motor stresses can stabilize initially floppy networks, extending the range of critical behavior to a broad regime of network connectivities below the marginal point. Away from this regime, or at high stress, motors give rise to a linear increase in stiffness with stress. Finally, we demonstrate that our results are captured by a simple, constitutive scaling relation highlighting the important role of nonaffine strain fluctuations as a susceptibility to motor stress.

DOI: [10.1103/PhysRevLett.109.238101](https://doi.org/10.1103/PhysRevLett.109.238101)

PACS numbers: 87.16.Ka, 62.20.de, 83.10.Tv, 83.60.Df

The mechanical properties of cells are regulated in part by internal stresses generated actively by molecular motors in the cytoskeletal filamentous actin network [1]. On a larger scale, collective motor activity allows the cell to contract the surrounding extracellular matrix, consisting also of biopolymer networks. Experiments show that such active contractility dramatically affects network elasticity, both in reconstituted intracellular *F*-actin networks with myosin motors [2–5] and in extracellular matrices with contractile cells [6]. The dynamics and elasticity of active biopolymer networks have been studied theoretically using long-wavelength hydrodynamic approaches [7] as well as affine models [8–10]. These approaches, however, fail to describe highly disordered networks. There is also experimental evidence that cytoskeletal networks may be unstable or only marginally stable in the absence of motor activity [11]. In such cases, networks are expected to be governed by highly nonuniform, soft or floppy modes of deformation that may lead to a fundamental breakdown or failure of continuum elasticity [12]. Importantly, motor-induced contractile stresses can be expected to couple to these soft modes [13], giving rise to a nonlinear elastic response that is distinct from the nonlinearities arising from single fiber elasticity that have been considered in previous models. Moreover, such a coupling to local soft modes of the network may call into question the equivalence of internal (motor) and external stress, a tacit assumption in the analysis of recent *in vitro* experiments [2,4].

Here, we introduce a simple model to study the effects of motor generated stresses on the elastic properties of disordered fiber networks. Networks are formed by cross-linked straight fibers with linear stretching and bending elasticity. These fibers are organized on a face centered cubic (fcc) lattice in which a certain fraction of the bonds can randomly be removed. This allows us to explore a wide range of network connectivities, $0 \leq z \leq 12$. Motor

activity is introduced by contractile, static, and strain-independent force dipoles acting between neighboring network nodes. We find that motors can stabilize the elastic response of otherwise floppy, unstable networks. The motor stress also controls the mechanics of stable networks above a characteristic threshold, in the vicinity of which the network exhibits critical strain fluctuations. We develop a quantitative effective medium theory (EMT) to describe the elastic response of these systems. Interestingly, the network's stiffness is controlled by a coupling of the motor induced stresses to the strain fluctuations. This coupling gives rise to anomalous regimes at the stability thresholds, at which network criticality is reflected in both divergent strain fluctuations and anomalous dependences of the network mechanics on stress. In these critical regimes, the shear modulus depends nonlinearly on both motor stress and single filament elasticity [6,13–15]. Interestingly, this dependence on internal motor stress differs qualitatively from that of an applied external stress.

A key parameter that characterizes fiber networks is the mean coordination number, z . Other network properties that have been found to affect the elastic properties of such networks include a jamming geometry [16] or a divergence of the average fiber length [17,18], neither of which is considered here. Although the network is connected above a threshold $z_{\text{cond}} \simeq 2$, it only becomes rigid above a higher rigidity threshold $z_b \simeq 3.4$ [12]. This threshold is due to the bending rigidity of the individual fibers and it lies below the central-force rigidity threshold, $z_{\text{CF}} \simeq 6$, for a spring-only network. In general, when some fraction of the bonds are under stress, additional *constraints* are introduced [19]. More formally, these constraints appear as scalar terms in the Hamiltonian [20] that can shift the various rigidity thresholds in the system. In random spring networks, for example, this can be realized by applying finite network deformations; this has been

studied in spring networks [21–23] where the actual rigidity threshold shifts continuously to lower values with the applied external strain. Under such external deformations, the internal stress is free to adopt the most favorable distribution. By contrast, motors impose a fixed distribution of internal stress, which may lead to a qualitatively different network mechanics.

To provide insight into the elasticity of fibrous networks with contractile *internal* stresses, we use a model of fibers organized on a fcc lattice. By removing lattice bonds with a probability $1 - p$, we tune the average coordination number, $z = Zp$, where the maximum connectivity $Z = 12$ for the undiluted lattice. Motors are introduced as contractile force dipoles and are inserted randomly with a probability q . The fibers are modeled as linear elastic beams with a stretching modulus μ and bending rigidity κ . Using units in which $\ell_0 = \mu = 1$, the total energy can be written as

$$H = \frac{1}{2} \sum_{\langle ij \rangle} P_{ij} (|\mathbf{r}_{ij}| - 1)^2 + \frac{\kappa}{2} \sum_{\langle ij k \rangle} P_{ij} P_{jk} \left(\frac{\mathbf{r}_{ij} \times \mathbf{r}_{jk}}{|\mathbf{r}_{ij}| |\mathbf{r}_{jk}|} \right)^2 + f \sum_{\langle ij \rangle} Q_{ij} |\mathbf{r}_{ij}| \quad (1)$$

where, $\mathbf{r}_{ij} = \mathbf{r}_i - \mathbf{r}_j$ and \mathbf{r}_i denotes the position of i th node, and $P_{ij} = 1$ for present bonds or $P_{ij} = 0$ for removed bonds. The first sum extends over neighboring pairs of vertices. The crosslinks themselves do not contribute a torsional stiffness and, thus, the second sum only extends over *coaxial* nearest neighbor bonds on the same fiber. The last term represents the work performed by the motors, where $Q_{ij} = 1$ if a motor acts between nodes i and j and $Q_{ij} = 0$ otherwise.

To develop a mean-field, EMT that captures the disordered nature of this model—including internal stresses—we extend the theory for the linear mechanical response of disordered spring networks [24–26]. In our EMT approach we ignore the bending contribution ($\kappa = 0$), allowing us to circumvent the difficulties involved in an EMT with three-point bending interactions [12,27,28]. Our EMT is based on a mapping between the disordered network and an ordered one with an effective elastic constant, yet with the same underlying lattice geometry and under the same internal stress as the original disordered system, denoted by σ_M . The effective elastic constant, $\tilde{\mu}(\sigma_M)$, is determined by a self-consistency condition; the local distortion in the effective medium induced by replacing a bond, selected randomly from the disordered system, should vanish on average. For a general disordered network this procedure yields an implicit expression for the effective stretch modulus [29]

$$\int_0^\infty \frac{\mu_{ij} - \tilde{\mu}(\sigma_M)}{\mu_{EM} + \mu_{ij} - \tilde{\mu}(\sigma_M)} \mathcal{P}(\mu_{ij}) d\mu_{ij} = 0, \quad (2)$$

where μ_{EM}^{-1} equals the displacement of a bond in the unperturbed effective medium due to a unit force acting

along the bond, μ_{ij} is the stretching modulus between nodes i and j , and $\mathcal{P}(\mu_{ij})$ is the probability density of the moduli in the disordered system. For the case of a diluted fcc lattice considered here, $\mathcal{P}(\mu_{ij}) = p\delta(\mu_{ij} - 1) + (1 - p)\delta(\mu_{ij})$, we find an effective shear modulus

$$G_{EM} = \frac{5\sqrt{2}}{72} \tilde{\mu}(\sigma_M) + \frac{5}{6} \sigma_M, \quad (3)$$

where $\sigma_M = \sqrt{8}qf$ within the EMT.

While the full expression for $\tilde{\mu}(\sigma_M)$ is long [29], the scaling predictions of the EMT are simple. Even below the central-force isostatic point, z_{CF} , motor activity induces a finite shear modulus. Far from z_{CF} , $G \sim G_0 + \sigma_M$, where G_0 is the shear modulus of the unstressed network [30]. By contrast, close to z_{CF} there is an anomalous scaling regime $G \sim \sigma_M^{1/2} \mu^{1/2}$.

To test the implications of the EMT and effects of a finite bending rigidity, we simulate fiber networks with $\kappa > 0$. The shear modulus, G , is determined by applying a shear strain along the 111-plane using Lees-Edwards periodic boundary conditions and energy minimization by a conjugate gradient algorithm [31]. First, we consider the high motor density limit $q \simeq 1$. The dependence of G on motor stress and connectivity is shown in Figs. 1(a) and 1(b). Except where G is governed by κ , e.g., for connectivities between z_b and z_{CF} and $\sigma_M \ll \kappa$, the EMT prediction is in good quantitative agreement with the numerical results

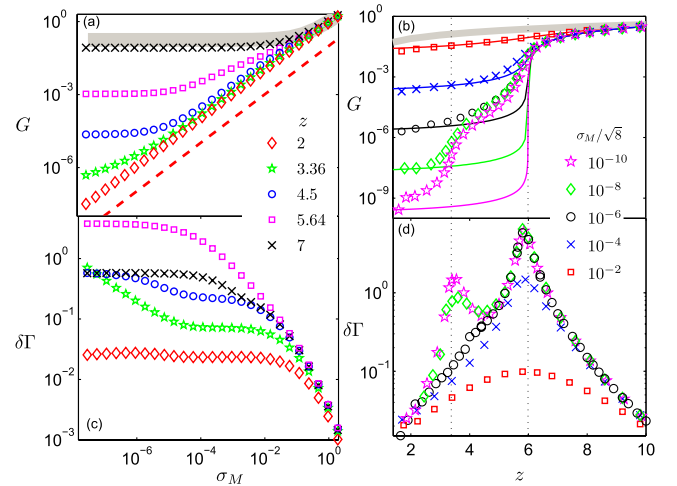


FIG. 1 (color online). (a) Shear modulus vs motor stress for various values of z . Symbols represent the numerical data. The dashed line represents a linear dependence and the grey region indicates affine predictions for all presented coordination numbers (see Ref. [29] for comparison with EMT). (b) G vs z for various values of σ_M . Symbols represent numerical data. Thin, solid lines represent EMT predictions. The grey line indicates the affine prediction. (c) The differential nonaffinity $\delta\Gamma$ vs motor stress for various values of z . (d) $\delta\Gamma$ vs z for various values of σ_M and for $\kappa = 10^{-5}$. Dotted vertical lines in (b),(d) represent the two rigidity thresholds, z_b and z_{CF} .

over a range of network parameters. This is to be expected, since the EMT does not account for fiber bending stiffness. The comparison is shown in Fig. 1(b) and Ref. [29].

Moreover, in the vicinity of z_{CF} for $\sigma_M \gg \kappa$, we find a mixed regime, in which

$$G \sim \mu^{1-y'} \sigma_M^{y'} \quad (4)$$

with $y' \simeq 0.4$, whereas $y' = 1/2$ in the EMT (Fig. 2). Such mixed regimes are known to arise in the vicinity of stability thresholds when additional, stabilizing interactions or fields are added, in such diverse systems as resistor and unstressed elastic networks [12,22,32]. In this model, motor stress can be thought of as an external field that stabilizes floppy networks. Consistent with this, we find an additional anomalous regime near the bending rigidity threshold, where

$$G \sim \kappa^{1-y} \sigma_M^y \quad (5)$$

with $y \simeq 0.6$ (Fig. 2).

We gain additional physical insight into the elastic properties of active networks with a scaling argument to estimate the amount of work that is performed by the motors when the system is sheared. The characteristic deformation of a single bond in such a network will be such that it avoids energetically costly stretching contributions.

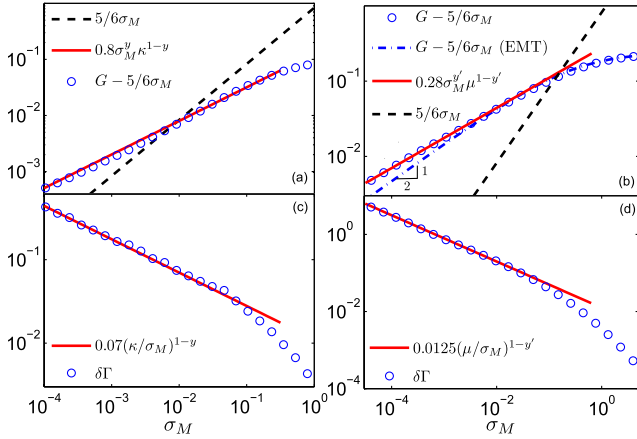


FIG. 2 (color online). Demonstration of the anomalous regimes in Eqs. (4), (5), and (8). (a) Shear modulus separated into the linear part, $5/6\sigma_M$ (dashed line), and $G - 5/6\sigma_M$ (circles) is shown for $z = 3.35$ (close to the bending rigidity percolation point, $z_b \simeq 3.36$) and $\kappa = 10^{-2}$. In the low stress limit, $G - 5/6\sigma_M$ scales as σ_M^y with $y \simeq 0.6$ (solid line). (b) The same analysis as in (a) for $z = 5.9$ (close to the central-force rigidity percolation point, $z_{CF} \simeq 5.64$) and $\kappa = 0$. In the low stress limit, $G - 5/6\sigma_M$ scales as $\sigma_M^{y'}$ with $y' \simeq 0.4$ (solid line), in contrast to the mean-field prediction (indicated by the dash-dotted line) with $y' = 1/2$. (c) The nonaffinity $\delta\Gamma$ (circles) for the same set of parameters as in (a). At low stress, this scales as σ_M^{y-1} (solid line). (d) The nonaffinity $\delta\Gamma$ (circles) for the same set of parameters as in (b). At low stress, this scales as $\sigma_M^{y'-1}$ (solid line).

Such deformations are oriented perpendicularly to the direction of the bond: the *nonaffine* contribution to this deformation can be estimated by $\delta u_{\perp} \sim \gamma\sqrt{\delta\Gamma}$, where the differential nonaffinity parameter is defined as,

$$\delta\Gamma = \frac{1}{\gamma^2} \langle (\delta\mathbf{u}_k - \delta\mathbf{u}_k^{\text{aff}})^2 \rangle_k. \quad (6)$$

Here $\delta\mathbf{u}_k$ is the displacement of node k under an infinitesimal external shear γ , $\delta\mathbf{u}_k^{\text{aff}}$ is the affine prediction and the average is taken over all network nodes. Interestingly however, this is not the only relevant contribution to the deformation of the bond. The component of the *affine* deformation perpendicular to the bond does not contribute to bond-stretching energies to harmonic order and, thus, is not avoided. Importantly however, this deformation does contribute to the motor work. Therefore, the total work performed by the internal stress resulting from such deformations scales as $\delta W \sim \sigma_M \gamma^2 \delta\Gamma + \sigma_M \gamma^2$, implying the following relationship for the shear modulus:

$$G \sim G_0 + \sigma_M \delta\Gamma + \sigma_M. \quad (7)$$

The nonaffinity, $\delta\Gamma$, depends on system parameters as shown in Figs. 1(c) and 1(d). As predicted by Eq. (7), we find that $G - G_0 - \frac{5}{6}\sigma_M$ vs $\sigma_M \delta\Gamma$ collapses onto a single line for all system sizes, as shown in Fig. 3(a). Interestingly, the scaling in Eq. (7) also suggests that $\delta\Gamma$ can be interpreted as a susceptibility of the shear modulus to internal stress. Consistent with this, $\delta\Gamma$ exhibits strong peaks close to both rigidity thresholds [Fig. 1(d)], which are critical points. At these points of marginal stability, we find that σ_M suppresses critical fluctuations, as shown by the marked reduction in $\delta\Gamma$ in Fig. 1(c) with increasing motor stress. This further supports the interpretation of σ_M as a field that takes the system away from criticality and suggests a power law dependence of $\delta\Gamma$ on σ_M . This dependence, taken together with Eq. (7), can account for the observed scaling of G in Eqs. (4) and (5) provided that

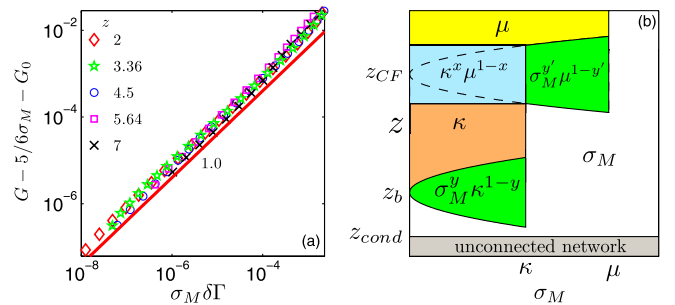


FIG. 3 (color online). (a) Collapse of the data presented on Fig. 1(a) based on Eq. (7). The red line shows a linear dependence. (b) The schematic phase diagram for the rigidity of random spring networks under an internal stress σ_M . For all the regimes governed by κ (low values of σ_M and intermediate values of z) the EMT is expected to fail.

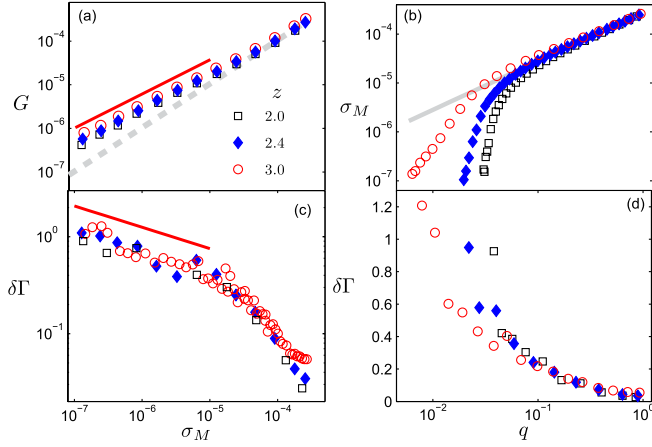


FIG. 4 (color online). The role of inhomogeneity in the motor distribution for different values of z [see legend in panel (a) for all plots]. (a) Shear modulus vs normal stress induced by the motors. Solid line represents the power law of 0.78, while the dashed line indicates the mean-field predictions. (b) The normal stress vs motor occupation probability q . Solid line represents the mean-field prediction, $\sigma_M = \sqrt{8}qf$. (c) The differential nonaffinity measure vs σ_M for the same parameters as in (a). The solid line represents the power law of -0.22 . (d) $\delta\Gamma$ vs q . For all the data in this figure $f = 10^{-4}$ and $\kappa = 10^{-5}$.

$$\delta\Gamma(z_b) \sim \left(\frac{\kappa}{\sigma_M}\right)^{1-y} \quad \text{and} \quad \delta\Gamma(z_{CF}) \sim \left(\frac{\mu}{\sigma_M}\right)^{1-y'} \quad (8)$$

To confirm this, we directly observe scaling of $\delta\Gamma$ consistent with Eq. (8) and the previously observed exponents y and y' , as shown in Figs. 2(c) and 2(d).

The schematic phase diagram for the high-motor density limit is shown in Fig. 3(b). Away from the stability thresholds the shear modulus scales linearly with the active stress. This is in contrast with the stiffening behavior of *externally* deformed networks, for which the dependence of the differential elastic modulus goes as the square root of the external stress [22,23]. Thus, there is not necessarily a quantitative correspondence between internally and externally stressed networks, in contrast to suggestions in prior work [4].

Finally, we explore the role of inhomogeneity in the distribution of active motors, which shows that critical behavior is not limited to the critical points associated with rigidity percolation. We model inhomogeneous motors by considering the range $q < 1$ for different values of z well below the rigidity percolation point, $z < z_b$. In this case the motors only induce a macroscopic stress when the motor density exceeds a z -dependent threshold, $q_c(z)$, as shown in Fig. 4(b). Importantly, the effective connectivity at this threshold remains well below the isostatic point. Concurrent with the development of a macroscopic stress, the network acquires a finite shear rigidity. Near the threshold q_c , the motor-induced stress falls significantly below the mean-field prediction ($\sigma_M = \sqrt{8}qf$) and

depends nonlinearly on q . Interestingly, in this regime ($\sigma_M \ll \sqrt{8}q_c f$) the nonaffine fluctuations become large [see Fig. 4(d)], diverging with motor stress with an exponent close to -0.22 , as shown in Fig. 4(c). Such a divergence, taken together with Eq. (7), implies an anomalous, sublinear exponent 0.78, in Fig. 4(a). This happens even when the mean coordination number of the network is well below the rigidity percolation point. Thus, criticality in the form of a divergent susceptibility is not limited to the marginal points, z_b and z_{CF} , but occurs over range of connectivities below z_{CF} .

This work demonstrates that motor activity controls the elastic properties of disordered networks by coupling to the differential nonaffine fluctuations in the deformation field. This coupling makes elastic deformations more affine and stabilizes the network. Far from the elastic critical points this coupling leads to linear stiffening as a function of the motors stress, as has been observed in several studies of prestressed elastic networks [33,34]. However, G scales sublinearly with the global stress induced by motors. Similar stress-stiffening of floppy networks below marginal stability is also found beyond a threshold in the motor density, indicating a surprising generality of critical fluctuations and divergent susceptibility for systems below the usual rigidity percolation point.

This work was supported in part by FOM/NWO and in part by a Lewis-Sigler fellowship (C. P. B.). The authors thank B. Shklovskii and L. Jawerth for helpful discussions.

- [1] J. Howard, *Mechanics of Motor Proteins and the Cytoskeleton* (Sinauer Associates, Sunderland, 2001).
- [2] D. Mizuno, C. Tardin, C. F. Schmidt, and F. C. MacKintosh, *Science* **315**, 370 (2007).
- [3] P. M. Bendix, G. H. Koenderink, D. Cuvelier, Z. Dogic, B. N. Koeleman, W. M. Briehner, C. M. Field, L. Mahadevan, and D. A. Weitz, *Biophys. J.* **94**, 3126 (2008).
- [4] G. H. Koenderink, Z. Dogic, F. Nakamura, P. M. Bendix, F. C. MacKintosh, J. H. Hartwig, T. P. Stossel, and D. A. Weitz, *Proc. Natl. Acad. Sci. U.S.A.* **106**, 15 192 (2009).
- [5] D. Gordon, A. Bernheim-Groswasser, C. Keasar, and O. Farago, *Phys. Biol.* **9**, 026005 (2012).
- [6] W. A. Lam, O. Chaudhuri, A. Crow, K. D. Webster, T.-D. Li, A. Kita, J. Huang, and D. A. Fletcher, *Nat. Mater.* **10**, 61 (2011).
- [7] K. Kruse, J. F. Joanny, F. Jülicher, J. Prost, and K. Sekimoto, *Eur. Phys. J. E* **16**, 5 (2005).
- [8] F. C. MacKintosh and A. J. Levine, *Phys. Rev. Lett.* **100**, 018104 (2008).
- [9] T. B. Liverpool, M. C. Marchetti, J.-F. Joanny, and J. Prost, *Europhys. Lett.* **85**, 18007 (2009).
- [10] Y. Shokef and S. A. Safran, *Phys. Rev. Lett.* **108**, 178103 (2012).
- [11] Y. Cai, O. Rossier, N. C. Gauthier, N. Biais, M.-A. Fardin, X. Zhang, L. W. Miller, B. Ladoux, V. W. Cornish, and M. P. Sheetz, *J. Cell Sci.* **123**, 413 (2010).

- [12] C.P. Broedersz, X. Mao, T.C. Lubensky, and F.C. MacKintosh, *Nat. Phys.* **7**, 983 (2011).
- [13] C.P. Broedersz and F.C. MacKintosh, *Soft Matter* **7**, 3186 (2011).
- [14] A. Ehrlicher and J.H. Hartwig, *Nat. Mater.* **10**, 12 (2011).
- [15] P. Chen and V.B. Shenoy, *Soft Matter* **7**, 355 (2011).
- [16] W.G. Ellenbroek, Z. Zeravcic, W. van Saarloos, and M. van Hecke, *Europhys. Lett.* **87**, 34 004 (2009).
- [17] C.P. Broedersz, M. Sheinman, and F.C. MacKintosh, *Phys. Rev. Lett.* **108**, 078102 (2012).
- [18] O. Stenull and T.C. Lubensky, [arXiv:1108.4328](https://arxiv.org/abs/1108.4328).
- [19] E.M. Huisman and T.C. Lubensky, *Phys. Rev. Lett.* **106**, 088301 (2011).
- [20] S. Alexander, *Phys. Rep.* **296**, 65 (1998).
- [21] W. Tang and M.F. Thorpe, *Phys. Rev. B* **37**, 5539 (1988).
- [22] M. Wyart, H. Liang, A. Kabla, and L. Mahadevan, *Phys. Rev. Lett.* **101**, 215501 (2008).
- [23] M. Sheinman, C.P. Broedersz, and F.C. MacKintosh, *Phys. Rev. E* **85**, 021801 (2012).
- [24] S. Feng, M.F. Thorpe, and E. Garboczi, *Phys. Rev. B* **31**, 276 (1985).
- [25] L.M. Schwartz, S. Feng, M.F. Thorpe, and P.N. Sen, *Phys. Rev. B* **32**, 4607 (1985).
- [26] X. Mao, N. Xu, and T.C. Lubensky, *Phys. Rev. Lett.* **104**, 085504 (2010).
- [27] M. Das, F.C. MacKintosh, and A.J. Levine, *Phys. Rev. Lett.* **99**, 038101 (2007).
- [28] X. Mao, O. Stenull, and T.C. Lubensky, [arXiv:1111.1751](https://arxiv.org/abs/1111.1751).
- [29] See Supplemental Material at <http://link.aps.org/supplemental/10.1103/PhysRevLett.109.238101> for the EMT calculation of the effective stretching modulus.
- [30] In all scaling relationships with additive contributions, unknown numerical prefactors are omitted.
- [31] W.H. Press, S.A. Teukolsky, W.T. Vetterling, and B.P. Flannery, *Numerical Recipes in C: The Art of Scientific Computing* (Cambridge University Press, New York, 1992), 2nd ed.
- [32] J.P. Straley, *J. Phys. C* **9**, 783 (1976).
- [33] B. Budiansky and E. Kimmel, *J. Appl. Mech.* **54**, 351 (1987).
- [34] D. Stamenovic and M. Coughlin, *J. Biomech. Eng.* **122**, 39 (2000).